Loss of huntingtin function slows synaptic vesicle endocytosis in striatal neurons from the httQ140/Q140 mouse model of Huntington's disease

Neurobiology of Disease 134 (2020) 104637

Contents lists available at ScienceDirect

Neurobiology of Disease

journal homepage: www.elsevier.com/locate/ynbdi

Loss of huntingtin function slows synaptic vesicle endocytosis in striatal neurons from the $htt^{Q140/Q140}$ mouse model of Huntington's disease

Robyn L. McAdam[a], Andrew Morton[a,1], Sarah L. Gordon[a,2], Julia F. Alterman[b,c], Anastasia Khvorova[b,c], Michael A. Cousin[a,*], Karen J. Smillie[a,*]

[a] Centre for Discovery Brain Sciences, Hugh Robson Building, University of Edinburgh, Edinburgh EH8 9XD, Scotland, UK
[b] RNA Therapeutics Institute, University of Massachusetts Medical School, Worcester, MA, USA
[c] Department of Molecular Medicine, University of Massachusetts Medical School, Worcester, MA, USA

ARTICLE INFO

Keywords:
Neuron
Synapse
Endocytosis
Vesicle
Huntington's disease
Endosome
Clathrin
Neurodegeneration

ABSTRACT

Huntington's disease (HD) is caused by CAG repeat expansion within the *HTT* gene, with the dysfunction and eventual loss of striatal medium spiny neurons a notable feature. Since medium spiny neurons receive high amounts of synaptic input, we hypothesised that this vulnerability originates from an inability to sustain presynaptic performance during intense neuronal activity. To test this hypothesis, primary cultures of either hippocampal or striatal neurons were prepared from either wild-type mice or a knock-in HD mouse model which contains 140 poly-glutamine repeats in the huntingtin protein ($htt^{Q140/Q140}$). We identified a striatum-specific defect in synaptic vesicle (SV) endocytosis in $htt^{Q140/Q140}$ neurons that was only revealed during high frequency stimulation. This dysfunction was also present in neurons that were heterozygous for the mutant *HTT* allele. Depletion of endogenous huntingtin using hydrophobically-modified siRNA recapitulated this activity-dependent defect in wild-type neurons, whereas depletion of mutant huntingtin did not rescue the effect in $htt^{Q140/Q140}$ neurons. Importantly, this SV endocytosis defect was corrected by overexpression of wild-type huntingtin in homozygous $htt^{Q140/Q140}$ neurons. Therefore, we have identified an activity-dependent and striatum-specific signature of presynaptic dysfunction in neurons derived from pre-symptomatic HD mice, which is due to loss of wild-type huntingtin function. This presynaptic defect may render this specific neuronal subtype unable to operate efficiently during high frequency activity patterns, potentially resulting in dysfunctional neurotransmission, synapse failure and ultimately degeneration.

1. Introduction

Neurotransmitter release is a tightly controlled event, relying on the synchronous coupling of activity-dependent calcium influx to synaptic vesicle (SV) fusion (Sudhof, 2012). This process can be difficult to sustain however, since SVs are highly limited within a typical small central nerve terminal (Schikorski and Stevens, 2001; Wilhelm et al., 2014). To maintain the fidelity of neurotransmission, SVs are recycled locally within the presynapse, with both SV cargo and membrane reformed into fusion-competent SV by endocytosis (Cousin, 2017; Saheki and De Camilli, 2012). When SV endocytosis is perturbed, neurotransmission is disrupted (Chen et al., 2003; Koh et al., 2004; Koo et al., 2015; Shupliakov et al., 1997).

Huntington's Disease (HD) is a monogenic disorder caused by a variable CAG expansion in exon 1 of the *HTT* gene, resulting in the expressed huntingtin protein (htt) containing an extended poly-glutamine tract. The disease is characterized by chorea followed by hypokinesis, thought to result from a specific degeneration of medium spiny neurons (MSNs) in the striatum (Vonsattel et al., 1985). However, a molecular explanation for the loss of this specific neuronal subtype is currently undetermined.

An emerging theme in a number of degenerative conditions is the

Abbreviations: HD, Huntington's Disease; htt, huntingtin; mhtt, mutant huntingtin; MSN, medium spiny neuron; SV, synaptic vesicle; hsiRNA, hydrophobically-modified short interfering RNA; NTC, non-targeting control; DIV, days in vitro; ROI, region of interest; syp-pH, synaptophysin-pHluorin; AP-2, Adaptor protein complex 2.

* Corresponding authors.
E-mail addresses: M.Cousin@ed.ac.uk (M.A. Cousin), K.Smillie@ed.ac.uk (K.J. Smillie).
[1] Present address - School of Physics and Astronomy, University of St Andrews, North Haugh, St Andrews, Scotland, KY16 9SS.
[2] Present address - Florey Institute of Neuroscience and Mental Health, The University of Melbourne, 30 Royal Parade, Parkville, 3052, Victoria, Australia.

https://doi.org/10.1016/j.nbd.2019.104637
Received 26 October 2018; Received in revised form 23 August 2019; Accepted 9 October 2019
Available online 12 October 2019
0969-9961/

premise that early presynaptic dysfunction plays a contributory role towards later pathological outcomes (Waites and Garner, 2011). In this regard, striatal MSNs receive a high level of excitatory synaptic input to maintain them in their "up" state (Milnerwood and Raymond, 2010; Wolf et al., 2005). This suggests that the polyglutamine expansion in mutant htt (mhtt) may result in an intrinsic inability of MSNs to sustain neurotransmitter release during such input, rendering them unable to maintain the fidelity of neurotransmission with downstream synaptic partners. Consistent with this, dysfunctional striatal transmission with its target areas has been observed in electrophysiological studies in animal models (Barry et al., 2018) and terminal loss (presumably preceded by dysfunction) has been recorded in human neuropathological studies (Albin et al., 1992; Reiner et al., 1988).

Wild-type htt is enriched at central nerve terminals (DiFiglia et al., 1995; Yao et al., 2014), suggesting it performs a role in presynaptic function that may be disrupted on poly-glutamine expansion in HD. We tested the hypothesis that poly-glutamine expansion of mhtt results in the intrinsic dysfunction of specific neuronal subtypes that would only be revealed by elevated neuronal activity. To achieve this, we examined how high frequency input impacted on presynaptic function in primary neuronal cultures derived from the $htt^{Q140/Q140}$ knock-in mouse (Menalled et al., 2003). We discovered an activity-dependent defect in SV endocytosis that was specific to striatal neurons. Importantly, this defect was a consequence of loss of wild-type htt function and was observed in heterozygous neurons, providing potential disease relevance. The activity-dependent nature of this SV endocytosis defect suggests that the intrinsic dysfunction of striatal HD neurons may result in an inability to sustain neurotransmission during high frequency input, resulting in synaptic failure and ultimately their degeneration.

2. Materials and methods

2.1. Materials

Synaptophysin-pHluorin (Syp-pH) was provided by Prof. L. Lagnado (University of Sussex). The htt expression plasmid (human Htt-Q22-pcDNA3.1) provided by Cure Huntington's Disease Initiative (CHDI) via the Coriell Institute for Medical Research (Camden, NJ). $Htt^{Q140/Q140}$ knockin mice were provided by CHDI via The Jackson Laboratory. The following antibodies were used: mouse anti-α-adaptin (for immunoprecipitation, Thermo Scientific MA1–064), mouse anti-Htt (1:8000 for WB; Merck MAB2166) and mouse anti-β-actin (1:250000 for WB; Sigma-Aldrich A3854). Rabbit anti-Htt (1:250; Abcam 109115), chicken anti-GFP (1:2000; Abcam 13970) and Alexa-conjugated secondary antibodies (1:500) were purchased from Life Technologies (Paisley, UK). Secondary antibodies for WB (IRDye 800CW anti-mouse; LI-COR 927–32210, 1:10000) and Odyssey blocking buffer (927–4000) were purchased from LI-COR Biosciences (Cambridge, UK). Neurobasal media, B-27 supplement, penicillin/streptomycin, Minimal Essential Medium, Dulbecco's Minimal Essential Medium: Nutrient Mixture F12, Lipofectamine 2000, phosphate buffered salts, were obtained from Life Technologies. Papain was from Lorne laboratories (Reading, UK). APV and CNQX were from Abcam (Cambridge, UK). All other reagents were obtained from Sigma-Aldrich (Poole, UK).

2.2. Oligonucleotide synthesis, deprotection and purification

Hydrophobic modification of siRNA enables efficient internalization by primary neurons without requirement for standard transfection methods (Alterman et al., 2015). HsiRNA against htt (HTT10150) and NTC hsiRNA were based on a previously identified HTT functional targeting site (Alterman et al., 2015). The compounds were asymmetric, composed of a 15-nucleotide long duplex region with a single-stranded 3′ extension on the guide strand. All bases were modified using alternating 2′-*O*-methyl /2′-fluoro modification pattern with additional 14 phosphorothioates incorporated (Table 1). The 3′ end of the passenger strand was conjugated to a hydrophobic teg-Chol (tetraethylene glycol cholesterol).

Oligonucleotides were synthesized on an OligoPilot100 Synthesizer. Both sense and antisense strands were cleaved and deprotected using 40% aq.methylamine at 65 °C for 15 min. The oligonucleotide solutions were then cooled in a freezer and dried under vacuum in a Speedvac. The resulting pellets were suspended in water. The final purification of oligonucleotides was performed on an Agilent Prostar System (Agilent, Santa Clara, CA) equipped with a Hamilton HxSil C18 column (150 × 21.2). The pure oligonucleotides were collected, desalted by size-exclusion chromatography using a Sephadex G25 and lyophilized. The identity of oligonucleotides was established by LC-MS analysis on an Agilent 6530 accuratemass Q-TOF LC/MS (Agilent technologies, Santa Clara, CA). The purified strands were duplexed and duplex formation and purity were confirmed by gel electrophoresis.

2.3. Mouse colony maintenance and management

All animal work was performed in accordance with the UK Animal (Scientific Procedures) Act 1986, under Project and Personal License authority and was approved by the Animal Welfare and Ethical Review Body at the University of Edinburgh. Specifically, all animals were killed by schedule 1 procedures in accordance with UK Home Office Guidelines. In-house colonies of either wild-type C57Bl/6J mice or $htt^{Q140/Q140}$ knockin mice (which express a chimeric mouse/human exon 1 inserted into the murine htt gene containing a 140 CAG expansion (Menalled et al., 2003)) on a C57Bl/6J background were maintained as homozygotes. For specific experiments using heterozygotes, these mice were crossed to obtain $htt^{Q140/+}$ offspring. Gene sequencing to confirm CAG repeat length in $htt^{Q140/Q140}$ mice was performed by Laragen (Culver City, US).

2.4. Primary neuronal culture

Primary cultures of striatal neurons were prepared, since selective loss of striatal MSNs is a key feature of HD (Milnerwood and Raymond, 2010). Hippocampal neurons were prepared as a control (Zhang et al., 2015). Either dissociated primary hippocampal- or striatal-enriched cultures were generated from both male and female E16–18 mouse embryos. Dissected tissue was digested in papain (0.3 U / ml) supplemented phosphate buffered saline (PBS) at 37 °C for 20 min. Papain was then removed and replaced with Dulbecco's Modified Eagle Medium: Nutrient Mixture F-12 supplemented with 10% *w/v* foetal bovine serum and triturated to obtain a single-cell suspension. The suspension was centrifuged for 5 min at 347*g*. The supernatant was discarded and the pellet resuspended in Neurobasal medium supplemented with 2% B-27 supplement, 0.5 mM L-glutamine, and 1% *v*/v penicillin/streptomycin. Hippocampal and striatal neurons were plated at a density of 4×10^4 and 6.5×10^4 cells/coverslip respectively. Cells were plated onto a 50 µl laminin spot in the centre of a 25 mm coverslip pre-coated with poly-D-lysine in boric acid (100 mM, pH 8.5) within a 6-well plate. After 1 h, wells were flooded in the same Neurobasal media as above, and media was supplemented after 72 h with 1 µM cytosine β-d-arabinofuranoside to inhibit glial proliferation. In htt knockdown experiments, 0.5 µM of either hsiRNA or NTC was added to culture media after 7 days in vitro (DIV). All other transfections were performed after 7 or 8 DIV using 0.6–1.0 µg of DNA per plasmid and 2 µl of lipofectamine 2000 per well. Imaging experiments were performed at 13 to 15 DIV.

2.5. Imaging and analysis of pHluorin reporters

SV recycling was visualised using syp-pH. Syp-pH has a pH-sensitive GFP moiety (pHluorin) fused to an intraluminal loop of the SV protein synaptophysin (Granseth et al., 2006). The fluorescence of syp-pH is quenched by the acidic SV interior; however, during SV exocytosis its fluorescence is unquenched on encountering the neutral pH of the

Table 1
Modification of hsiRNA.

siRNA ID	Accession number	Strand	Sequence
$hsiRNA^{NTC}$	N/A	Sense	fU#mG#fA.mC.fA.mA.fAm.U.fA.mC.fG.mA.fU#mU#fA-TegChol
		Antisense	PmU#fA#mA.fU.mC.fG.mU.fA.mU.fU.mU.fG.mU#fC#mA#fA#mU#fC#mA#fU
$hsiRNA^{HTT}$	NM_002111	Sense	fC#mA#fG.mU.fA.mA.fA.mG.fA.mG.fA.mU.fU#mA#fA-TegChol
		Antisense	PmU#fU#mA.fA.mU.fC.mU.fC.mU.fU.mU.fA.mC#fU#mG#fA#mU#fA#mU#fA

Chemical modifications are designated as follows. "." – Phosphodiester bond, "#" – Phosphorothioate bond, "m" – 2'-O-Methyl, "f" – 2'-Fluoro, "P" – 5' Phosphate, "TegChol" –Tetraethylene glycol (teg)-Cholesterol.

extracellular medium. Syp-pH is then re-quenched during endocytosis and subsequent SV acidification.

Coverslips containing primary cultures were mounted in a Warner imaging chamber (RC-21BRFS) embedded with parallel platinum wires (6 mm apart). Cultures were subjected to continuous perfusion in imaging buffer containing (in mM): 119 NaCl, 2.5 KCl, 2 $CaCl_2$, 2 $MgCl_2$, 25 HEPES, 30 glucose, 0.01 CNQX and 0.05 AP5, pH 7.4. Imaging was performed on a Zeiss Axio Observer D1 inverted epi-fluorescence microscope (Zeiss Ltd. Germany) using a x40 1.3 NA oil immersion objective at room temperature unless otherwise indicated. Images were acquired at 4 s intervals using a Hamamatsu Orca-ER camera (Hamamatsu, Japan). Cultures were electrically stimulated with specific trains of electrical field stimulation (either 300 pulses delivered at 10 Hz or 400 pulses delivered at 40 Hz; both 100 mA, 1 ms pulse width). At the end of the experiment, cultures were perfused with alkaline imaging buffer (50 mM NH_4Cl substituted for 50 mM NaCl) to reveal total pHluorin fluorescence.

Wavelength settings for syp-pHluorin were 480 nm excitation and > 525 nm emission. Offline processing was performed using Fiji is just ImageJ (FIJI) software (Schindelin et al., 2012). Regions of interest (ROIs) of identical size were placed over axonal nerve terminals (Fig. 1A-D) and the fluorescence intensity was monitored over time using the Time Series Analyser V2 plugin. The change in activity-dependent pHluorin fluorescence was calculated as $\Delta F/F_0$ using Microsoft Excel. Traces were normalised to the peak during stimulation or to total pHluorin fluorescence (by normalising to the peak response in the presence of alkaline buffer). In all cases, n refers to the number of independent coverslips examined.

2.6. Immunofluorescence

Nerve terminal htt expression was assessed using immunofluorescence. After 13–15 DIV, neurons were washed twice with PBS (pH 7.4) and fixed for 15 min at room temperature in PBS containing 4% paraformaldehyde. Cultures were incubated for 5 min with PBS containing 50 mM ammonium chloride, followed by two sequential 5 min PBS washes. Cells were permeabilized by incubation in 0.1% Triton X-100 in PBS for 10 min, followed by three PBS washes, and blocking for 1 h with 2% BSA in PBS. Primary and secondary antibodies were each diluted in 1% BSA in PBS and incubated with cells for 1 h at room temperature and washed with three sequential PBS washes before and after secondary incubation. Images were acquired on a Zeiss Axio Observer D1 microscope using 480 nm excitation and > 510 emission to visualise Alexa-488, and 550 nm excitation and > 575 nm emission to visualise Alexa-568. Expression levels of htt were determined by using FIJI software to measure the mean fluorescence intensity of neuronal cell bodies. The mean fluorescence of a transfected neuron cell body was normalised to the average of the mean fluorescence of the neighbouring untransfected neurons within the same field of view. Experimental n represents data from independent coverslips.

2.7. Immunoprecipitation

Forebrain synaptosomes were prepared from either adult wild-type or $htt^{Q140/Q140}$ mice by differential centrifugation as previously described (Anggono et al., 2006). Synaptosomes were lysed in ice-cold lysis buffer (1% Triton X-100, 150 mM NaCl, 25 mM Tris pH 7.4, 1 mM EDTA, 1 mM EGTA, 20 mg/ml leupeptin, 1 mM phenylmethylsulfonyl fluoride and protease inhibitor mix) for 15 min and then centrifuged for 5 min at 20,000 *g*. Supernatants from this lysate were incubated with Protein G-coupled Sepharose beads and 5 μg of α-adaptin antibody with rotation overnight. Beads were washed with lysis buffer twice, with lysis buffer supplemented with 500 mM NaCl once, again with lysis buffer and finally with 20 mM Tris (pH 7.4). Bound proteins were then eluted in SDS sample buffer (67 mM SDS, 2 mM EGTA, 9.3% glycerol, 12% β-mercaptoethanol, bromophenol blue, 67 mM Tris, pH 7.4), boiled for 5 min at 95 °C and analysed by Western blotting. Experimental n represents data from 6 separate immunoprecipitations.

2.8. Western blotting

Western blotting was used to assess immunoprecipitations and htt knockdown efficiency. Approximately 150,000 neurons were plated on individual coverslips, which were lysed at 13–15 DIV directly in SDS sample buffer. Samples were boiled for 5 min at 95 °C and resolved using SDS-PAGE (4–20% gel, Bio-Rad), and transferred to nitrocellulose membrane using a Bio-Rad Mini Trans-Blot Cell transfer apparatus. The membrane was incubated for 1 h in Odyssey blocking buffer before a 1 h incubation rotating at room temperature in blocking buffer containing 0.1% tween-20 and primary antibody. Four 5 min washes in blocking buffer occurred before and after 1 h incubation with secondary antibody. Protein bands were detected with an Odyssey scanner (800 nm channel) and quantified using FIJI software. Experimental n represents data from neuronal lysates derived from independent coverslips.

2.9. Experimental design and statistical analysis

All statistical analysis was performed in Graph Pad Prism 6.0. A one-way ANOVA with Tukey's post-test was used to compare more than two groups. A two-tailed student's t-test was performed when two groups were compared. The sample size (n) was taken to be either the number of independent experiments or individual coverslips as indicated above. All data are presented as mean values ± standard error of the mean (SEM).

3. Results

3.1. Establishment of an experimental system to interrogate presynaptic dysfunction in HD neurons

Dysfunctional synaptic transmission is one of the key events that precipitate a number of neurodegenerative disorders, sometimes termed synaptopathies (Brose et al., 2010; Waites and Garner, 2011), with HD included within this definition (Li et al., 2003; Milnerwood and Raymond, 2010; Rozas et al., 2010). In this study, we investigated whether presynaptic function was altered before overt pathological or motor symptoms of HD occurred, to determine whether this may contribute to disease initiation.

SV recycling was monitored in primary cultures derived from either

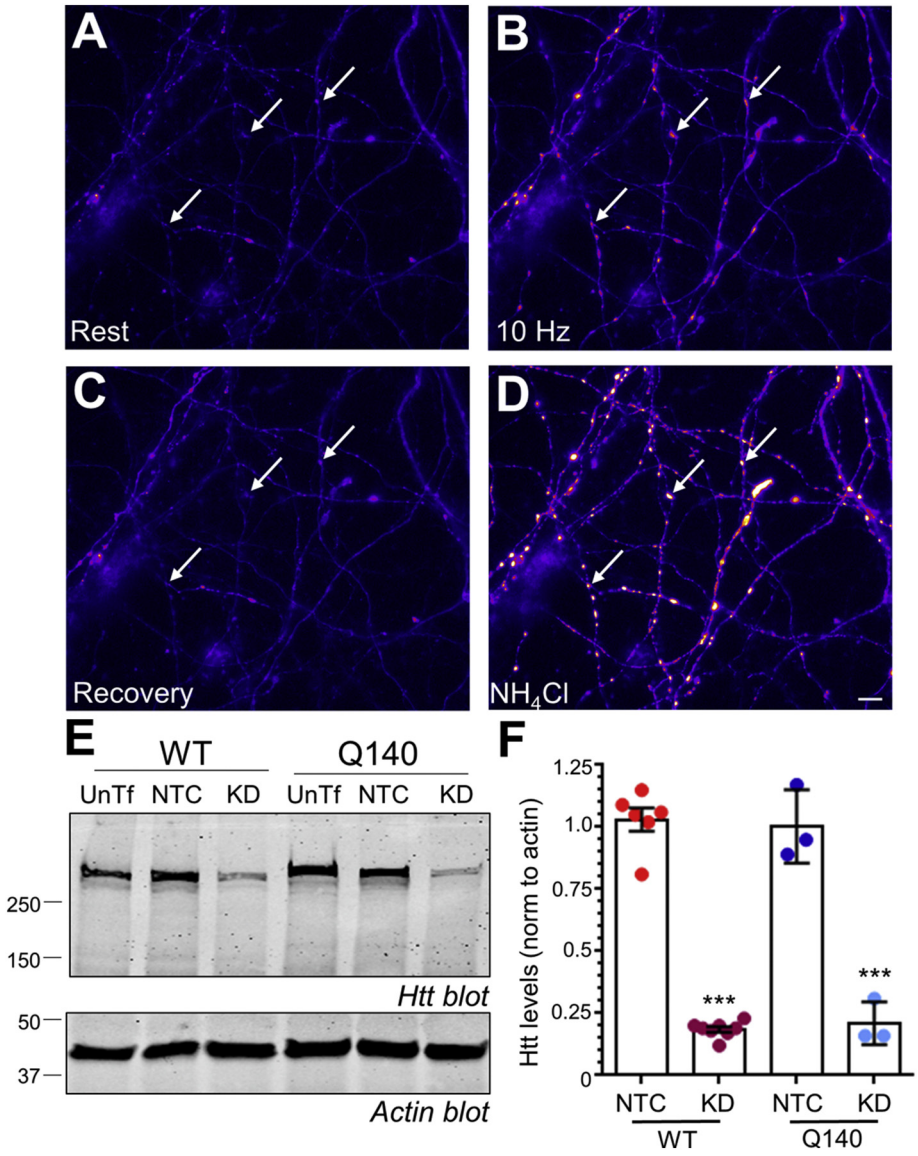

Fig. 1. – *Establishment of an experimental platform to study the effect of htt loss and gain of function in wild-type and htt$^{Q140/Q140}$ neurons*. Primary cultures of wild-type (WT) hippocampal neurons were transfected with synaptophysin-pHluorin (syp-pH) 7 days prior to fluorescence imaging. Cultures were challenged with a train of 300 electrical field stimuli delivered at 10 Hz followed by a pulse of ammonium chloride buffer (NH_4Cl). (A-D) Representative images showing the syp-pH response either before (Rest, A), during (10 Hz, B) or after (Recovery, C) the stimulus train. The syp-pH signal in response to NH_4Cl challenge is displayed in D. Arrows indicate typical responsive puncta. Scale bar represents 10 µm. (E) Representative Western blot of htt levels from neuronal lysates derived from either wild-type (WT) or htt$^{Q140/Q140}$ (Q140) hippocampal cultures after 7 days in the presence of 0.5 µM of htt hsiRNA (KD) or non-targeting control (NTC). Lysates from untransfected (UnTf) neurons are also displayed. A representative actin blot from the same membrane is displayed. (F) Bar graph displays the average extent of htt or mhtt expression (normalised to actin loading controls) ± SEM as a proportion of transfected controls. Red points indicate WT NTC, maroon points WT KD, dark blue points Q140 NTC and light blue points Q140 KD (WT NTC $n = 6$, WT KD $n = 8$; Q140 NTC $n = 3$, Q140 KD n = 3; one-way ANOVA to WT NTC, *** = $p < .001$). (For interpretation of the references to colour in this figure legend, the reader is referred to the web version of this article.)

wild-type mice or a preclinical model of HD, the htt$^{Q140/Q140}$ knock-in mouse. This mouse expresses a chimeric mouse/human exon 1, containing a CAG repeat of approximately 140, inserted into the murine *HTT* gene, resulting in a large polyglutamine expansion in the expressed htt protein (Menalled et al., 2003). Primary cultures of striatal neurons were examined since a key feature of HD is the selective loss of striatal MSNs (Milnerwood and Raymond, 2010). Hippocampal neurons were examined in parallel as a control.

Presynaptic function was monitored using the genetically encoded reporter syp-pH. Syp-pH reports the pH of its immediate environment by virtue of a pH-sensitive GFP moiety (pHluorin) fused to an intraluminal loop of the SV protein synaptophysin (Granseth et al., 2006). When syp-pH is present inside SVs, its fluorescence is quenched by the acidic lumenal pH; however, on translocation to the plasma membrane its fluorescence is unquenched due to the neutral pH of the extracellular medium. Neuronal activity results in syp-pH dequenching due to SV fusion (exocytosis), resulting in an increase in fluorescence (Fig. 1A,B). After neuronal activity terminates, the syp-pH fluorescence signal is re-quenched by SV acidification after its retrieval by SV endocytosis (Fig. 1C). The kinetics of SV endocytosis can be estimated by monitoring the rate of fluorescence decrease post-stimulation (Kavalali and Jorgensen, 2014), since SV acidification is not rate limiting in this process (Atluri and Ryan, 2006; Egashira et al., 2015; Granseth et al., 2006).

To determine whether any observed phenotype in htt$^{Q140/Q140}$ neurons was due to a loss of wild-type htt function or a toxic gain of mhtt function, we employed hydrophobically-modified siRNA (hsiRNA) which was designed to deplete both wild-type htt and mhtt (Alterman et al., 2015). The rationale for this approach was that a phenotype originating from a toxic gain of mhtt function would be corrected by depletion of mutant htt in htt$^{Q140/Q140}$ neurons. In contrast, if a loss of htt function was responsible for any phenotype, depletion of htt in wild-type cultures should mimic the phenotype of htt$^{Q140/Q140}$ neurons.

We first confirmed the knockdown efficiency of both wild-type htt and mhtt in their respective cultures. The targeting hsiRNA efficiently and equally depleted both htt in wild-type neurons and mhtt in htt$^{Q140/Q140}$ neurons to approximately 20% of untransfected controls (Fig. 1E,F). In contrast, there was no depletion of either htt or mhtt compared to transfected neurons in wild-type and htt$^{Q140/Q140}$ hippocampal neurons that were treated with a non-targeting control (NTC) hsiRNA (Fig. 1E,F). Therefore, we established an experimental system that will 1) identify dysfunction in SV recycling in HD neurons, and 2) whether any observed dysfunction is a result of a loss of normal htt function or a toxic gain of mhtt function.

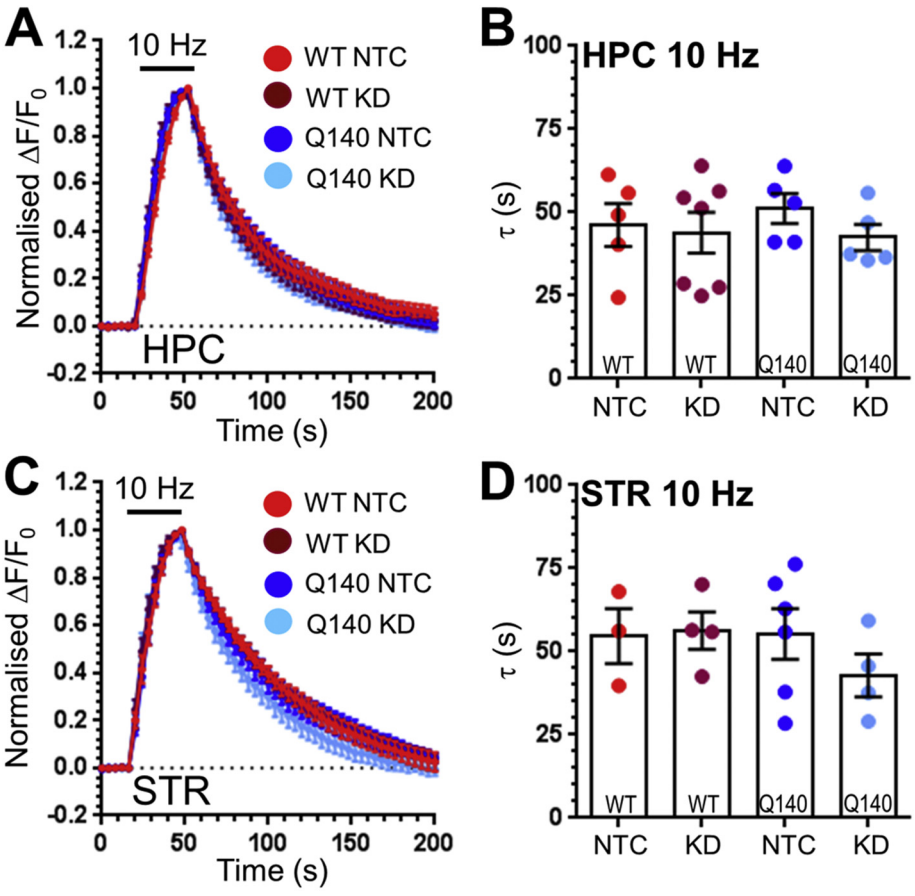

Fig. 2. – *SV endocytosis is unaffected in htt$^{Q140/Q140}$ neurons at low stimulation frequencies*. Primary cultures of either hippocampal (HPC) or striatal (STR) neurons generated from either wild-type (WT) or htt$^{Q140/Q140}$ (Q140) mice were transfected with synaptophysin-pHluorin (syp-pH). In addition, cultures were treated with 0.5 μM of htt hsiRNA (KD) or a non-targeting control (NTC) for 7 days previously. Cultures were challenged with a train of 300 electrical field stimuli delivered at 10 Hz followed by a pulse of ammonium chloride buffer (NH_4Cl). (A,C) Traces display the time course of the average fluorescent syp-pH response normalised to the peak of stimulation ($\Delta F/F_0$ ± SEM) in all conditions for either HPC (A) or STR (C). Red traces indicate WT NTC, maroon traces WT KD, dark blue traces Q140 NTC and light blue traces Q140 KD. Bar indicates period of stimulation. (B,D) Quantification of the time constant (τ) for the syp-pH fluorescence decrease ± SEM (HPC WT $n = 5$ NTC, n = 6 KD; HPC Q140, n = 5 NTC, n = 5 KD: STR WT n = 3 NTC, $n = 4$ KD; STR Q140 n = 6 NTC, n = 4 KD independent experiments). One-way ANOVA all not significant. (For interpretation of the references to colour in this figure legend, the reader is referred to the web version of this article.)

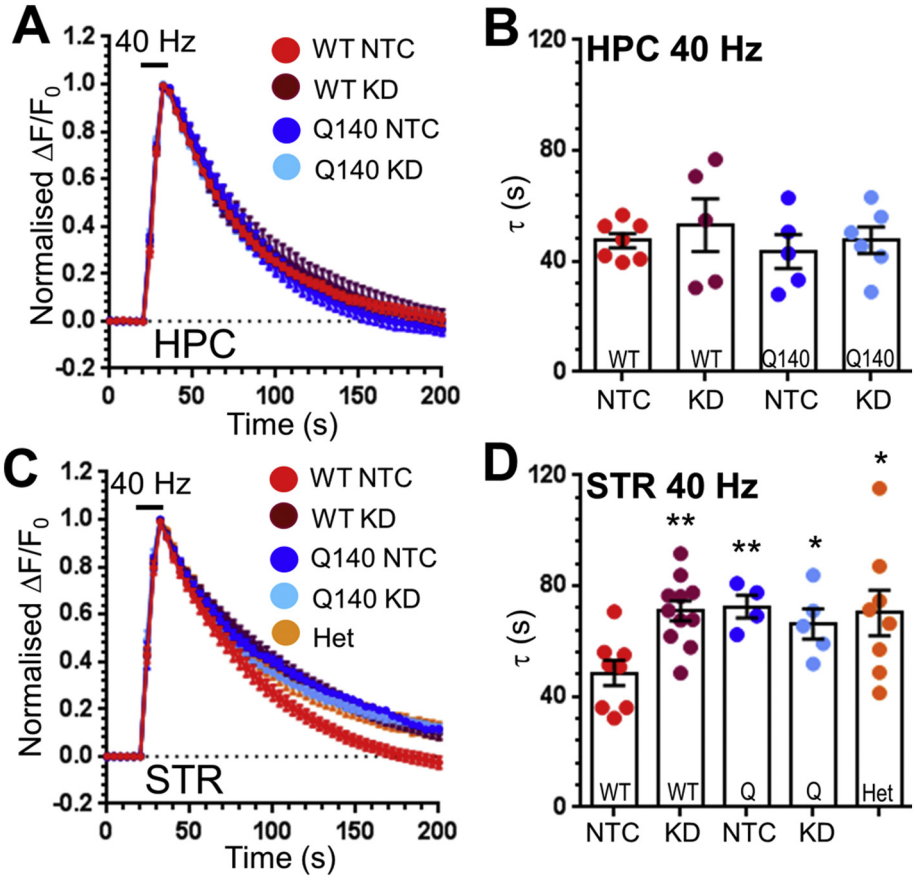

Fig. 3. – *SV endocytosis is disrupted in striatal htt$^{Q140/Q140}$ neurons specifically during high neuronal activity*. Primary cultures of either hippocampal (HPC) or striatal (STR) neurons generated from either wild-type (WT), htt$^{Q140/Q140}$ (Q140) or htt$^{Q140/+}$ (Het) mice were transfected with synaptophysin-pHluorin (syp-pH). In addition cultures were treated with 0.5 μM of htt hsiRNA (KD) or a non-targeting control (NTC) where indicated for 7 days previously. Cultures were challenged with a train of 400 electrical field stimuli delivered at 40 Hz followed by a pulse of ammonium chloride buffer. (A,C) Traces display the time course of the average fluorescent syp-pH response normalised to the peak of stimulation ($\Delta F/F_0$ ± SEM) in all conditions for either HPC (A) or STR (C). Red traces indicate WT NTC, maroon traces WT KD, dark blue traces Q140 NTC, light blue traces Q140 KD and orange traces Het. Bar indicates period of stimulation. (B,D) Quantification of the time constant (τ) for the syp-pH fluorescence decrease ± SEM (HPC WT $n = 7$ NTC, $n = 5$ KD; HPC Q140, n = 5 NTC, $n = 6$ KD: STR WT n = 7 NTC, $n = 11$ KD; STR Q140 n = 4 NTC, n = 5 KD; STR Het $n = 8$). One-way ANOVA against WT NTC, ** = $p < .01$; * = $p < .05$. (For interpretation of the references to colour in this figure legend, the reader is referred to the web version of this article.)

3.2. SV recycling has no obligatory requirement for htt

We first determined whether SV endocytosis was altered during low frequency (10 Hz, 30 s) stimulation in either wild-type or $htt^{Q140/Q140}$ neurons that were treated with hsiRNA (either targeting or NTC). Importantly, delivery of hsiRNA did not impact on presynaptic function (Supplementary Fig. 1). When wild-type and $htt^{Q140/Q140}$ neurons were compared, there was no genotype-dependent difference in either the extent (estimated by the return of the syp-pH signal to baseline, Fig. 2A,C) or kinetics (estimated by the time constant [Tau, τ] of syp-pH fluorescence decay, Fig. 2B,D) of SV endocytosis for either hippocampal or striatal neurons. Furthermore, depletion of either htt from wild-type neurons or mhtt from $htt^{Q140/Q140}$ neurons had no impact on either the extent or kinetics of SV endocytosis for both hippocampal and striatal neurons (Fig. 2). There was no effect of any manipulation on the peak syp-pH response, indicating no effect on evoked SV fusion events (Supplementary Fig. 2). These experiments indicate that SV endocytosis is unaffected during low levels of neuronal activity in $htt^{Q140/Q140}$ neurons derived from different brain regions. Importantly, it also reveals that htt is dispensable for SV endocytosis during low frequency stimulation, since its depletion in wild-type neurons has no impact on this parameter.

3.3. $Htt^{Q140/Q140}$ knockin neurons display a striatum-specific, activity-dependent defect in SV endocytosis due to loss of wild-type htt function

Our initial hypothesis was that poly-glutamine expansion of mhtt would result in the selective dysfunction of specific neuronal subtypes that are challenged by elevated neuronal activity. This is particularly pertinent for striatal MSNs, which receive a high frequency of input (Milnerwood and Raymond, 2010). Therefore, we next assessed the impact of increasing the stimulation frequency to 40 Hz (400 field stimuli) on SV endocytosis. When the evoked syp-pH response was monitored in hippocampal cultures treated with NTC hsiRNA, no genotype-dependent alterations in either the extent or kinetics of SV endocytosis was observed (Fig. 3A,B). In contrast, striatal $htt^{Q140/Q140}$ NTC hsiRNA-treated cultures displayed a slowing in the kinetics of SV endocytosis after high frequency stimulation when compared to wild-type NTC hsiRNA-treated controls (Fig. 3C,D). The extent of SV endocytosis was unaffected in striatal $htt^{Q140/Q140}$ neurons, since the syp-pH response did return to baseline (Supplementary Fig. 3). This striatum-specific, activity-dependent defect was also apparent when these experiments were performed at physiological temperatures (Fig. 4). This is an important control, since it has been proposed that the activation of different SV endocytosis modes is temperature-dependent (Chanaday and Kavalali, 2018; Delvendahl et al., 2016; Watanabe et al., 2014). Thus, striatal neurons from $htt^{Q140/Q140}$ mice display a selective defect in the kinetics of SV endocytosis that is only revealed during elevated neuronal activity.

We next determined whether this activity-dependent, striatum-specific dysfunction in SV endocytosis was due to either a loss of wild-type htt function or a toxic gain of mhtt function. When htt was depleted with hsiRNA in either wild-type or $htt^{Q140/Q140}$ hippocampal neurons, no effect on SV endocytosis was observed after high frequency stimulation, in agreement with the lack of genotype effect in these neurons (Fig. 3A,B). However, when htt was depleted in wild-type striatal neurons, a significant slowing in the kinetics of SV endocytosis was observed, very similar to that observed in NTC-treated $htt^{Q140/Q140}$ striatal neurons (Fig. 3C,D). When mutant htt was depleted in $htt^{Q140/Q140}$ striatal neurons, no additional retardation in SV endocytosis kinetics was observed compared to either NTC-treated $htt^{Q140/Q140}$ striatal neurons or hsiRNA-treated wild-type striatal neurons (Fig. 3D). The extent of SV endocytosis was unaffected, as evidenced by the return to baseline of the syp-pH response (Supplementary Fig. 3). Thus, the activity-dependent defect in SV endocytosis observed exclusively in $htt^{Q140/Q140}$ striatal neurons, is due to a loss of wild-type htt function and not a toxic gain of mhtt function.

To address the possibility that the observed slowing of SV endocytosis in either $htt^{Q140/Q140}$ striatal neurons or hsiRNA-treated wild-type neuronal cultures was due to altered SV exocytosis, we examined the evoked peak height as a proportion of the total SV pool. The total SV pool is revealed by dequenching the syp-pH signal with an ammonium chloride buffer after completion of the experiment (Fig. 1D). To confirm that the evoked peak height was an accurate measure of SV exocytosis, we applied the V-type ATPase antagonist bafilomycin A1. This procedure arrests SV acidification after endocytosis, and therefore reveals the total number of SVs that visit the plasma membrane during a stimulus train, since endocytosis cannot be detected (Sankaranarayanan and Ryan, 2001). There was no difference in the peak syp-pH response between neurons treated with or without bafilomycin A1 during a 40 Hz train of stimuli (bafilomycin A1 minus 39.7 ± 3.4% of total SV pool $n = 7$; plus 34.9 ± 5.3%, $n = 3$, students t-test $p = .47$, Fig. 5A). This indicates that very few SVs are retrieved during this high frequency stimulus train, in agreement with previous work (Kokotos et al., 2018). When the syp-pH peak heights evoked by 40 Hz stimulation trains were examined, no change was observed across any experimental

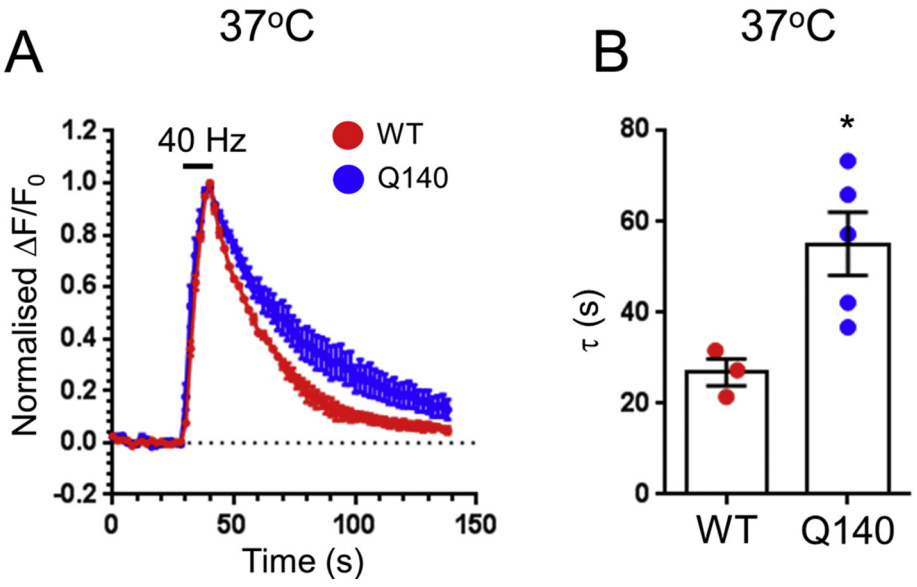

Fig. 4. – *SV endocytosis is disrupted in striatal $htt^{Q140/Q140}$ neurons during high neuronal activity at physiological temperatures.* Primary cultures of striatal neurons generated from either wild-type (WT) or $htt^{Q140/Q140}$ (Q140) mice were transfected with synaptophysin-pHluorin (syp-pH). Cultures were challenged with a train of 400 electrical field stimuli delivered at 40 Hz. (A) Traces display the time course of the average fluorescent syp-pH response normalised to the peak of stimulation (ΔF/F_0 ± SEM). Red traces indicate WT and blue traces indicate Q140. Bar indicates period of stimulation. (B) Quantification of the time constant (τ) for the syp-pH fluorescence decrease ± SEM (WT n = 3, Q140 n = 5). Students t-test * $p = .025$. (For interpretation of the references to colour in this figure legend, the reader is referred to the web version of this article.)

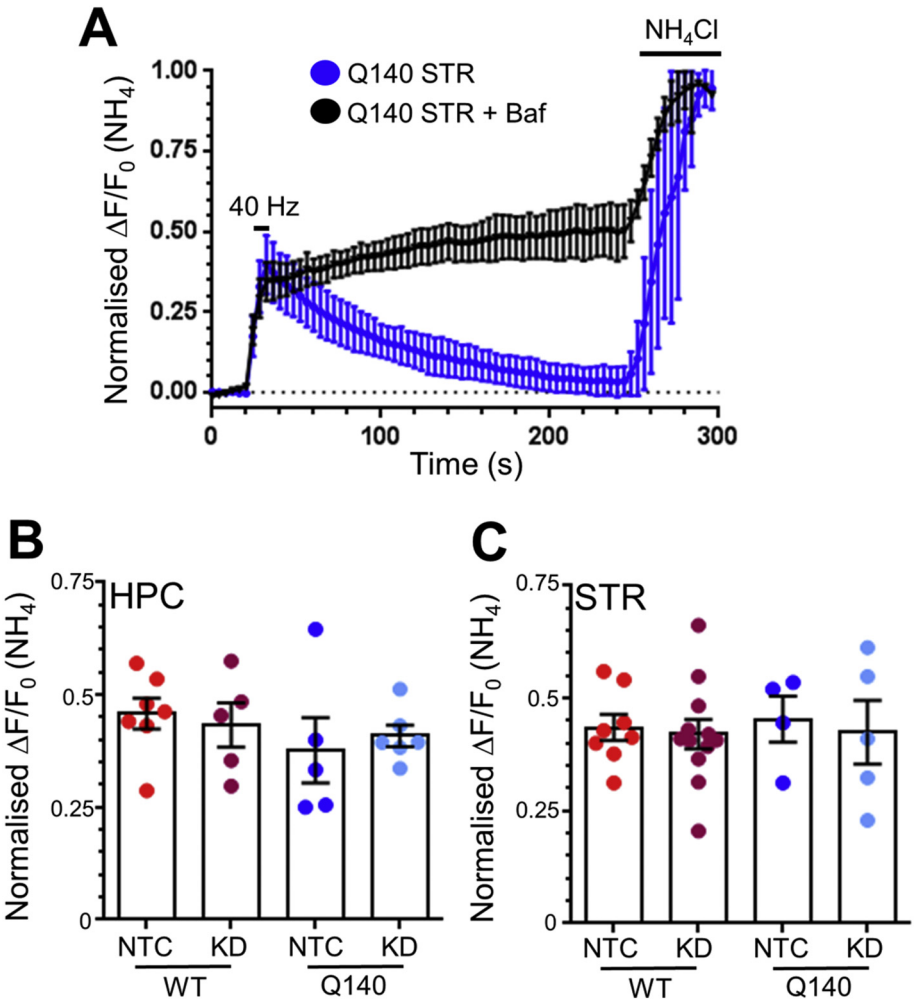

Fig. 5. – *SV exocytosis is unaffected in htt$^{Q140/Q140}$ neurons during high neuronal activity*. Primary cultures of either hippocampal (HPC) or striatal (STR) neurons generated from either wild-type (WT) or htt$^{Q140/Q140}$ (Q140) mice were transfected with synaptophysin-pHluorin (syp-pH). (A) Q140 STR neurons were challenged with a train of 400 electrical field stimuli delivered at 40 Hz followed by a pulse of ammonium chloride (NH_4Cl) buffer in either the presence (black trace) or absence (blue trace) of 1 μM bafilomycin A1 (Baf, which arrests SV acidification after endocytosis). The time course of the syp-pH response is displayed as a proportion of the total SV recycling pool (revealed by NH_4Cl) ± SEM (Q140 - Baf n = 6, Q140 + Baf n = 3). Bars indicate period of stimulation or application of NH_4Cl. (B,C) Cultures were treated with 0.5 μM of htt hsiRNA (KD) or a non-targeting control (NTC) for 7 days previously. Cultures were challenged with a train of 400 electrical field stimuli delivered at 40 Hz followed by a pulse of NH_4Cl buffer. Bar graphs display the extent of the syp-pH response in either HPC (B) or STR (C) neurons as a proportion of the total SV recycling pool (revealed by NH_4Cl) ± SEM. Red points indicate WT NTC neurons, maroon points WT KD, blue points Q140 NTC and light blue Q140 KD neurons. There was no significant difference in the evoked peak height for any stimulation condition or brain region (HPC WT n = 7 NTC, n = 5 KD; HPC Q140, n = 5 NTC, n = 6 KD: STR WT n = 7 NTC, n = 11 KD; STR Q140 n = 4 NTC, n = 5 KD, one-way ANOVA, all ns). (For interpretation of the references to colour in this figure legend, the reader is referred to the web version of this article.)

condition, genotype or neuronal subtype (Fig. 5B,C). Therefore, the observed defect in endocytosis in striatal neurons in unlikely to be a secondary consequence of altered exocytosis.

3.4. Wild-type htt expression corrects the activity-dependent SV endocytosis defect in striatal htt$^{Q140/Q140}$ neurons

We have discovered that loss of wild-type htt function precipitates a defect in SV endocytosis that is only revealed during intense neuronal activity in striatal htt$^{Q140/Q140}$ neurons. This suggests that the introduction of wild-type htt into htt$^{Q140/Q140}$ neurons may rescue presynaptic function. To determine this, we expressed wild-type htt (with a polyglutamine tract of 22, Q22-htt) in both wild-type and htt$^{Q140/Q140}$ culture systems. The level of Q22-htt expression was approximately 1:1 with endogenous mhtt in htt$^{Q140/Q140}$ cultures (Fig. 6A,B).

We next determined whether expression of wild-type htt could rescue the activity-dependent defect in SV endocytosis in htt$^{Q140/Q140}$ striatal neurons. The expression of Q22-htt in wild-type striatal neurons had no effect on the evoked syp-pH response (Fig. 6C,D), indicating that overexpression of wild-type htt is not deleterious to SV endocytosis. When Q22-htt was expressed in htt$^{Q140/Q140}$ striatal neurons, a full restoration of kinetics to wild-type levels was observed (Fig. 6C,D). Thus, the activity-dependent defect in SV endocytosis in striatal htt$^{Q140/Q140}$ neurons is fully rescued by expression of Q22-htt, confirming loss of htt function as a key determinant in the perturbation of presynaptic performance in this HD system.

3.5. Heterozygous htt$^{Q140/+}$ neurons display striatum-specific, activity-dependent defects in SV endocytosis

We have revealed a striatum-specific and activity-dependent defect in SV endocytosis in htt$^{Q140/Q140}$ neurons, which is due to a loss of wild-type htt function. However, HD patients typically have only one copy of the mutant htt allele (Tyebji and Hannan, 2017), therefore it is important for disease relevance to determine whether this defect also occurs in heterozygous htt$^{Q140/+}$ neurons. To investigate this, we challenged striatal htt$^{Q140/+}$ neurons with a train of high frequency stimuli and monitored the syp-pH response. A significant slowing of SV endocytosis was observed, with the time constant of syp-pH fluorescence decay comparable to that of either htt$^{Q140/Q140}$ neurons or wild-type neurons where htt had been depleted via hsiRNA (Fig. 3C,D). Therefore, this striatum-specific activity-dependent defect in SV endocytosis also occurs in the heterozygous condition, suggesting it may have clinical relevance.

4. Discussion

We have identified a striatum-specific defect in SV endocytosis that results from a loss of wild-type htt function in neurons derived from a pre-symptomatic HD mouse model. This defect was only revealed during intense neuronal activity, suggesting that loss of wild-type htt function results in an inability of htt$^{Q140/Q140}$ neurons to sustain their normal function during these conditions. This defect was also observed in heterozygous neurons, suggesting it may have disease relevance. Finally, we were able to rescue SV endocytosis in striatal htt$^{Q140/Q140}$

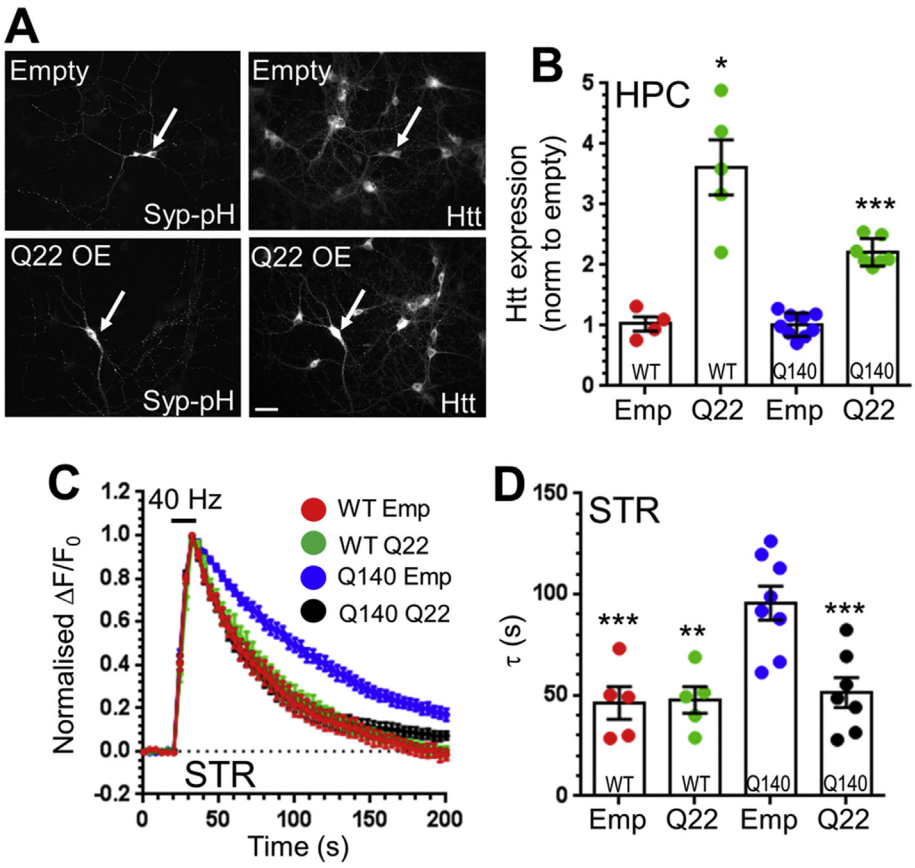

Fig. 6. – *Q22-htt expression rescues the activity-dependent SV endocytosis defect in striatal htt$^{Q140/Q140}$ neurons*. (A,B) Primary cultures from the hippocampus (HPC) of either wild-type (WT) or Htt$^{Q140/Q140}$ (Q140) mice were transfected with synaptophysin-pHluorin (syp-pH) and either empty pcDNA3.1 vector (Emp) or Q22-htt (Q22 OE) 7 days before fixation and immunostaining for both GFP (syp-pH) and htt. (A) Representative images show the syp-pH transfected neuron (arrow) and expression of htt. Scale bar indicates 20 μm. (B) Bar graph shows quantification of the level of htt expression as a percentage of untransfected neurons in the same field of view. Red points indicate WT Emp neurons, green points WT Q22, blue points Q140 Emp and green Q140 Q22 neurons (WT Emp n = 4, WT Q22 n = 5, Q140 Emp n = 9, Q140 Q22 n = 7). Two-tailed student's t-test * = p = .017 for WT and *** = p < .001 for Q140. (C,D) Primary striatal (STR) cultures from WT or Q140 mice were transfected with synaptophysin-pHluorin (syp-pH) and either Q22-htt (Q22) or an empty pcDNA3.1 vector (Emp). After 7 days cultures were stimulated with a single train of 400 electrical field stimuli at 40 Hz frequency. (C) Time course of the syp-pH response is displayed for either WT or Q140 neurons expressing either Emp or Q22-htt ($\Delta F/F_0$ ± SEM). Bar indicates period of stimulation. Red traces WT Emp neurons, green traces WT Q22, blue traces Q140 Emp and black traces Q140 Q22 neurons (D) Quantification of the time constant (τ) for the syp-pH fluorescence decrease (WT Emp n = 5, WT Q22 n = 6; Q140 Emp n = 9, Q140 Q22 n = 8 independent experiments, *** p < .001 against Q140 empty, one-way ANOVA). (For interpretation of the references to colour in this figure legend, the reader is referred to the web version of this article.)

neurons by introducing wild-type htt, confirming that this defect was a result of loss of wild-type htt function. These results reveal that presynaptic dysfunction occurs before clinical symptoms of HD manifest themselves and may be part of a cascade of deleterious synaptic events that culminate in synapse loss and degeneration of striatal neurons.

4.1. Choice of HD mouse model

A major rationale for our study was to identify presynaptic disease signatures at an age before any pathological, behavioral or motor correlate of HD are known to be apparent. We therefore chose the htt$^{Q140/Q140}$ knock-in mouse model for this study. This model system expresses full-length mhtt at endogenous levels, and only begins to display neuropathological abnormalities at 4 months and gait anomalies at 1 year (Hickey et al., 2008; Menalled et al., 2003). Therefore, we are confident that the activity-dependent defect in SV endocytosis observed in htt$^{Q140/Q140}$ neurons represents early presynaptic dysfunction that would precede HD symptoms. This contrasts with a number of other preclinical HD models, such as the R6/2 mouse, which displays a considerably accelerated disease progression, making a delineation between pre-symptomatic and symptomatic disease signatures more challenging. Such models (which overexpress mhtt exon 1 containing a large CAG repeat) display behavioral changes considerably earlier than full-length mhtt knock-in models and die within 4 months (Mangiarini et al., 1996). Moreover, nuclear inclusions appear in these models even before these symptoms appear (Morton et al., 2000). The loss of function in htt$^{Q140/Q140}$ neurons is not due to reduced presynaptic expression of mhtt, since it is detected at equivalent levels to wild-type neurons in these compartments (Valencia et al., 2013). Furthermore, no significant change in the expression levels of a series of selected presynaptic proteins was detected at 3 months (Valencia et al., 2013), suggesting that global alterations in presynaptic protein expression are not responsible for the defect in SV endocytosis identified in this study.

4.2. Activity-dependent and striatum-specific defect in SV endocytosis in HD neurons

We observe a selective vulnerability in SV endocytosis in striatal htt$^{Q140/Q140}$ neurons only during intense neuronal activity. This is likely to reflect slowing of clathrin-mediated endocytosis, since the clathrin inhibitor pitstop-2 almost eliminated the syp-pH downstroke after high frequency stimulation (Supplementary Fig. 4). It should also be noted that these cultures are enriched for MSNs, but will contain other neuronal subtypes. A slowing in the kinetics of the syp-pH response could be due to ineffective SV acidification, rather than retarded SV endocytosis (Watanabe et al., 2018). However, the absence of effect at low stimulation frequencies in striatal neurons and during both stimulation protocols in hippocampal neurons does not support this possibility. The molecular locus of this SV endocytosis defect is still unknown, however htt binds to numerous proteins that have direct roles in endocytosis, with polyglutamine expansion altering many of these interactions (Borgonovo et al., 2013; El-Daher et al., 2015; Engqvist-Goldstein et al., 2001; Li et al., 2008; Sittler et al., 1998). One specific association is with the clathrin adaptor protein AP-2, which is disrupted on polyglutamine expansion, resulting in a loss of function (Borgonovo et al., 2013). In agreement, we have also demonstrated a reduced interaction of mhtt with AP-2 in synaptosomes derived from htt$^{Q140/Q140}$ mice (Supplementary Fig. 5). Interestingly, AP-2 recruitment to the plasma membrane is disrupted in the striatum of HD mice, but not the cortex, cerebellum or hippocampus (Borgonovo et al., 2013). Therefore striatal htt$^{Q140/Q140}$ neurons may operate normally during low frequency input, however as the demand for SV endocytosis increases during elevated

activity, the impact of inefficient AP-2 recruitment via mhtt may become apparent. Alternatively, the inability of $htt^{Q140/Q140}$ striatal neurons to cope during intense neuronal activity may be a secondary consequence of an as-yet unidentified presynaptic process that retards SV endocytosis. In this scenario, most neurons are able to adapt their presynaptic function to compensate for the absence of this particular process during intense activity, however an intrinsic defect within $htt^{Q140/Q140}$ striatal neurons may render them specifically vulnerable. The identity of such a molecular or process deficit is currently unknown, however should be revealed through a systematic interrogation of the role of wild-type htt in presynaptic function.

A recent study revealed that presynaptic dysfunction occurred in an in vitro cortico-striatal co-culture system using $htt^{Q140/+}$ mice (Virlogeux et al., 2018). In this system, $htt^{Q140/+}$ cortical neurons displayed a decrease in the number of nerve terminals releasing glutamate regardless of their co-cultured synaptic partner ($htt^{Q140/+}$ or wild-type striatal neurons). Unfortunately, is it difficult to relate our work to this study for a number of reasons. These are; 1) SV recycling was not monitored in either cortical or striatal neurons; 2) cortical neurons were stimulated using a prolonged (5 min) exposure to inhibitory receptor antagonists (rather than brief trains of physiologically-relevant field stimuli); 3) the frequency of stimulation could not be modulated (due to the chemical depolarization) and 4) glutamate release was recorded using the genetically-encoded reporter GluSNFr (Marvin et al., 2013), the output from which was thresholded to produce a binary outcome – an active or non-active synapse. When one considers that the number of nerve terminals was reduced to a similar extent in cultures containing cortical $htt^{Q140/+}$ neurons, this suggests that the observed potential dysfunction was simply a result of less cortical synapses in the co-culture system.

4.3. Activity-dependent SV endocytosis defect in striatal HD neurons is due to htt loss of function

Individuals with HD are heterozygous for the mhtt allele, indicating a dominant pattern of inheritance. We observe a conservation of the activity-dependent SV endocytosis defect in striatal $htt^{Q140/+}$ neurons, highlighting a potential relevance for disease progression. The loss of function phenotype we observe suggests that it may result from htt haploinsufficiency. In support, heterozygous htt knockout mice display a series of cognitive, motor and pathological alterations that are comparable to those observed in knock-in models of HD (Menalled et al., 2009; Nasir et al., 1995; O'Kusky et al., 1999). Furthermore, conditional knockout of wild-type htt in adult brain forebrain results in extensive degeneration of a number of different neuronal subtypes, motor phenotypes and early mortality (Dragatsis et al., 2000). Alternatively, mhtt may still act in a dominant negative manner in heterozygotes to ablate wild-type htt function. In support, selective silencing of the mhtt allele was sufficient to restore normal brain-derived neurotrophic factor transport in HD patient cells (Drouet et al., 2014). Our observation that expression of wild-type htt fully rescues presynaptic function in $htt^{Q140/Q140}$ neurons argues against this, however it should be borne in mind that the expression levels of both wild-type htt and mhtt are approximately double when compared to the heterozygous condition in HD.

There has been considerable investment over the past decade in the development of a series of htt-lowering therapies (Caron et al., 2018). The logic of this approach is that the majority of deleterious effects observed are associated with a toxic gain of htt function. Our work, and that of others (Gauthier et al., 2004), reveal that loss of wild-type htt function also causes neuronal dysfunction and this should be considered in htt-lowering strategies. It also reveals that there is a relatively tight therapeutic window, since a reduction in wild-type htt expression from approximately 100% (in corrected $htt^{Q140/Q140}$ neurons, Fig. 6B) to 50% (in $htt^{Q140/+}$ neurons) results in presynaptic dysfunction.

Typically, slowed SV endocytosis results in a decrease in neurotransmission, which is due to a short-term depletion in SV numbers (Chen et al., 2003; Koh et al., 2004; Koo et al., 2015; Shupliakov et al., 1997). How might this alteration in SV endocytosis translate into altered striatal output in HD? MSNs have two specific outputs, the direct (projecting to the substantia nigra pars reticulata) or indirect (projecting to the external globus pallidus) pathway (Cepeda et al., 2014; Galvan et al., 2012; Rangel-Barajas and Rebec, 2016). MSNs of the indirect pathway appear to be particularly vulnerable in HD, which is proposed to lead to the observed chorea (Albin et al., 1992; Reiner et al., 1988). In addition, comparative studies of the two pathways suggest that MSNs of the indirect pathway fire at higher frequencies when injected with the same current as direct pathway MSNs (Gertler et al., 2008; Kreitzer and Malenka, 2007). The disproportionate excitability of these GABAergic MSNs may therefore result in decreased inhibitory drive though the indirect pathway, due to slowed SV endocytosis. Recent studies indicate that activation of indirect MSNs resulted in increased responses of direct pathway MSNs in HD mouse models (Barry et al., 2018), suggesting dysfunctional SV retrieval may contribute towards this increased communication. Directly addressing this hypothesis will be challenging, however the advent of new genetic and optogentic tools to dissect these pathways (Barry et al., 2018; Galvan et al., 2012) may provide a potential future research avenue.

5. Conclusions

The genetic cause and the progression of HD have been known for 20 years (Tyebji and Hannan, 2017; Zuccato and Cattaneo, 2014). However, the key molecular events that precipitate the degeneration of striatal MSNs and movement disorders remain unclear. An emerging view is that an intrinsic susceptibility of specific subtypes of neurons may render them progressively vulnerable to repeated insult or stressors, culminating in synapse failure and degeneration in later life. Repeated patterns of high frequency input may be such a physiological insult, rendering neurons that encounter such input at risk of dysfunctional neurotransmitter release and ultimately synaptic failure. The identification of key activity-dependent disease signatures in striatal neurons that occur before the manifestation of clinical symptoms is a promising avenue for future therapeutic intervention, since their early correction may ameliorate future synaptic loss and degeneration.

Acknowledgements

We thank Rona Wilson for assistance in the preparation of primary neuronal cultures. This work was supported by funding from Cure Huntington's Disease Initiative (CHDI, A-4390, A-11210 to MAC and KJS, A-6367 to AK), NIH (RO1GM10880302, S10 OD020012 to AK) and a studentship from the Biotechnology and Biological Sciences Research Council (to AM).

Appendix A. Supplementary data

Supplementary data to this article can be found online at https://doi.org/10.1016/j.nbd.2019.104637.

References

Albin, R.L., et al., 1992. Preferential loss of striato-external pallidal projection neurons in presymptomatic Huntington's disease. Ann. Neurol. 31, 425–430.
Alterman, J.F., et al., 2015. Hydrophobically modified siRNAs silence huntingtin mRNA in primary neurons and mouse brain. Mol Ther Nucleic Acids. 4, e266.
Anggono, V., et al., 2006. Syndapin I is the phosphorylation-regulated dynamin I partner in synaptic vesicle endocytosis. Nat. Neurosci. 9, 752–760.
Atluri, P.P., Ryan, T.A., 2006. The kinetics of synaptic vesicle reacidification at hippocampal nerve terminals. J. Neurosci. 26, 2313–2320.
Barry, J., et al., 2018. Striatal direct and indirect pathway output structures are differentially altered in mouse models of Huntington's disease. J. Neurosci. 38, 4678–4694.
Borgonovo, J.E., et al., 2013. Mutant huntingtin affects endocytosis in striatal cells by altering the binding of AP-2 to membranes. Exp. Neurol. 241, 75–83.
Brose, N., et al., 2010. Synaptopathy: dysfunction of synaptic function? Biochem. Soc. Trans. 38, 443–444.

Caron, N.S., et al., 2018. Therapeutic approaches to Huntington disease: from the bench to the clinic. Nat. Rev. Drug Discov. 17, 729–750.
Cepeda, C., et al., 2014. The role of dopamine in Huntington's disease. Prog. Brain Res. 211, 235–254.
Chanaday, N.L., Kavalali, E.T., 2018. Optical detection of three modes of endocytosis at hippocampal synapses. Elife. 7, e36097.
Chen, Y., et al., 2003. Formation of an endophilin-Ca^{2+} channel complex is critical for clathrin-mediated synaptic vesicle endocytosis. Cell. 115, 37–48.
Cousin, M.A., 2017. Integration of synaptic vesicle cargo retrieval with endocytosis at central nerve terminals. Front. Cell. Neurosci. 11, 234.
Delvendahl, I., et al., 2016. Fast, temperature-sensitive and Clathrin-independent endocytosis at central synapses. Neuron. 90, 492–498.
DiFiglia, M., et al., 1995. Huntingtin is a cytoplasmic protein associated with vesicles in human and rat brain neurons. Neuron. 14, 1075–1081.
Dragatsis, I., et al., 2000. Inactivation of Hdh in the brain and testis results in progressive neurodegeneration and sterility in mice. Nat. Genet. 26, 300–306.
Drouet, V., et al., 2014. Allele-specific silencing of mutant huntingtin in rodent brain and human stem cells. PLoS One 9, e99341.
Egashira, Y., et al., 2015. Monitoring of Vacuolar-type H^+ ATPase-mediated proton influx into synaptic vesicles. J. Neurosci. 35, 3701–3710.
El-Daher, M.T., et al., 2015. Huntingtin proteolysis releases non-polyQ fragments that cause toxicity through dynamin 1 dysregulation. EMBO J. 34, 2255–2271.
Engqvist-Goldstein, A.E., et al., 2001. The actin-binding protein Hip1R associates with clathrin during early stages of endocytosis and promotes clathrin assembly in vitro. J. Cell Biol. 154, 1209–1223.
Galvan, L., et al., 2012. Functional differences between direct and indirect striatal output pathways in Huntington's disease. J Huntingtons Dis. 1, 17–25.
Gauthier, L.R., et al., 2004. Huntingtin controls neurotrophic support and survival of neurons by enhancing BDNF vesicular transport along microtubules. Cell. 118, 127–138.
Gertler, T.S., et al., 2008. Dichotomous anatomical properties of adult striatal medium spiny neurons. J. Neurosci. 28, 10814–10824.
Granseth, B., et al., 2006. Clathrin-mediated endocytosis is the dominant mechanism of vesicle retrieval at hippocampal synapses. Neuron. 51, 773–786.
Hickey, M.A., et al., 2008. Extensive early motor and non-motor behavioral deficits are followed by striatal neuronal loss in knock-in Huntington's disease mice. Neuroscience. 157, 280–295.
Kavalali, E.T., Jorgensen, E.M., 2014. Visualizing presynaptic function. Nat. Neurosci. 17, 10–16.
Koh, T.W., et al., 2004. Dap160/intersectin acts as a stabilizing scaffold required for synaptic development and vesicle endocytosis. Neuron. 43, 193–205.
Kokotos, A.C., et al., 2018. Activity-dependent bulk endocytosis proteome reveals a key presynaptic role for the monomeric GTPase Rab11. Proc. Natl. Acad. Sci. U. S. A. 115, E10177–E10186.
Koo, S.J., et al., 2015. Vesicular Synaptobrevin/VAMP2 levels guarded by AP180 control efficient neurotransmission. Neuron 88, 330–344.
Kreitzer, A.C., Malenka, R.C., 2007. Endocannabinoid-mediated rescue of striatal LTD and motor deficits in Parkinson's disease models. Nature. 445, 643–647.
Li, J.Y., et al., 2003. Huntington's disease: a synaptopathy? Trends Mol. Med. 9, 414–420.
Li, X., et al., 2008. A function of huntingtin in guanine nucleotide exchange on Rab11. Neuroreport. 19, 1643–1647.
Mangiarini, L., et al., 1996. Exon 1 of the HD gene with an expanded CAG repeat is sufficient to cause a progressive neurological phenotype in transgenic mice. Cell. 87, 493–506.
Marvin, J.S., et al., 2013. An optimized fluorescent probe for visualizing glutamate neurotransmission. Nat. Methods 10, 162–170.
Menalled, L., et al., 2009. Systematic behavioral evaluation of Huntington's disease transgenic and knock-in mouse models. Neurobiol. Dis. 35, 319–336.
Menalled, L.B., et al., 2003. Time course of early motor and neuropathological anomalies in a knock-in mouse model of Huntington's disease with 140 CAG repeats. J. Comp. Neurol. 465, 11–26.
Milnerwood, A.J., Raymond, L.A., 2010. Early synaptic pathophysiology in neurodegeneration: insights from Huntington's disease. Trends Neurosci. 33, 513–523.
Morton, A.J., et al., 2000. Progressive formation of inclusions in the striatum and hippocampus of mice transgenic for the human Huntington's disease mutation. J. Neurocytol. 29, 679–702.
Nasir, J., et al., 1995. Targeted disruption of the Huntington's disease gene results in embryonic lethality and behavioral and morphological changes in heterozygotes. Cell. 81, 811–823.
O'Kusky, J.R., et al., 1999. Neuronal degeneration in the basal ganglia and loss of pallido-subthalamic synapses in mice with targeted disruption of the Huntington's disease gene. Brain Res. 818, 468–479.
Rangel-Barajas, C., Rebec, G.V., 2016. Dysregulation of Corticostriatal connectivity in Huntington's disease: a role for dopamine modulation. J Huntingtons Dis. 5, 303–331.
Reiner, A., et al., 1988. Differential loss of striatal projection neurons in Huntington disease. Proc. Natl. Acad. Sci. U. S. A. 85, 5733–5737.
Rozas, J.L., et al., 2010. Presynaptic dysfunction in Huntington's disease. Biochem. Soc. Trans. 38, 488–492.
Saheki, Y., De Camilli, P., 2012. Synaptic vesicle endocytosis. Cold Spring Harb. Perspect. Biol. 4, a005645.
Sankaranarayanan, S., Ryan, T.A., 2001. Calcium accelerates endocytosis of vSNAREs at hippocampal synapses. Nat. Neurosci. 4, 129–136.
Schikorski, T., Stevens, C.F., 2001. Morphological correlates of functionally defined synaptic vesicle populations. Nat. Neurosci. 4, 391–395.
Schindelin, J., et al., 2012. Fiji: an open-source platform for biological-image analysis. Nat. Methods 9, 676–682.
Shupliakov, O., et al., 1997. Synaptic vesicle endocytosis impaired by disruption of dynamin-SH3 domain interactions. Science. 276, 259–263.
Sittler, A., et al., 1998. SH3GL3 associates with the Huntingtin exon 1 protein and promotes the formation of polygln-containing protein aggregates. Mol. Cell 2, 427–436.
Sudhof, T.C., 2012. Calcium control of neurotransmitter release. Cold Spring Harb. Perspect. Biol. 4, a011353.
Tyebji, S., Hannan, A.J., 2017. Synaptopathic mechanisms of neurodegeneration and dementia: insights from Huntington's disease. Prog. Neurobiol. 153, 18–45.
Valencia, A., et al., 2013. Striatal synaptosomes from Hdh140Q/140Q knock-in mice have altered protein levels, novel sites of methionine oxidation, and excess glutamate release after stimulation. J Huntingtons Dis. 2, 459–475.
Virlogeux, A., et al., 2018. Reconstituting Corticostriatal network on-a-Chip reveals the contribution of the presynaptic compartment to Huntington's disease. Cell Rep. 22, 110–122.
Vonsattel, J.P., et al., 1985. Neuropathological classification of Huntington's disease. J. Neuropathol. Exp. Neurol. 44, 559–577.
Waites, C.L., Garner, C.C., 2011. Presynaptic function in health and disease. Trends Neurosci. 34, 326–337.
Watanabe, S., et al., 2014. Clathrin regenerates synaptic vesicles from endosomes. Nature. 515, 228–233.
Watanabe, S., et al., 2018. Synaptojanin and Endophilin mediate neck formation during ultrafast endocytosis. Neuron. 98, 1184–1197 e6.
Wilhelm, B.G., et al., 2014. Composition of isolated synaptic boutons reveals the amounts of vesicle trafficking proteins. Science. 344, 1023–1028.
Wolf, J.A., et al., 2005. NMDA/AMPA ratio impacts state transitions and entrainment to oscillations in a computational model of the nucleus accumbens medium spiny projection neuron. J. Neurosci. 25, 9080–9095.
Yao, J., et al., 2014. Huntingtin is associated with cytomatrix proteins at the presynaptic terminal. Mol. Cell. Neurosci. 63, 96–100.
Zhang, N., et al., 2015. Phosphorylation of synaptic vesicle protein 2A at Thr84 by casein kinase 1 family kinases controls the specific retrieval of Synaptotagmin-1. J. Neurosci. 35, 2492–2507.
Zuccato, C., Cattaneo, E., 2014. Huntington's disease. Handb. Exp. Pharmacol. 220, 357–409.